

Leptoquarks facing flavour tests and $b \rightarrow s\ell\ell$ after Moriond 2021

J. Kriewald ^a, C. Hati ^b, J. Orloff ^a and A. M. Teixeira ^a

^aLaboratoire de Physique de Clermont (UMR 6533), CNRS/IN2P3,
Univ. Clermont Auvergne, 4 Av. Blaise Pascal, F-63178 Aubière Cedex, France

^bPhysik Department T70, Technische Universität München,
James-Franck-Straße 1, D-85748 Garching, Germany

Abstract

In view of the emerging hints for the violation of lepton flavour universality in several B -meson decays, we conduct a model-independent study (effective field theory approach) of several well-motivated new physics scenarios. Taking into account the most recent LHCb data, we provide updates to Wilson coefficient fits for numerous popular new physics hypotheses. We also consider a promising model of vector leptoquarks, which in addition to explaining the B -meson decay anomalies ($R_{K^{(*)}}$ and $R_{D^{(*)}}$) would have an extensive impact for numerous flavour observables. We identify promising decay modes allowing to (indirectly) probe such an extension: these include positive signals (at Belle II or LHCb) for $\tau \rightarrow \phi\mu$, $B_{(s)}$ -meson decays to $\tau^+\tau^-$ and $\tau^+\mu^-$ (τ^+e^-) final states, as well as an observation of certain charged lepton flavour violation transitions at COMET and Mu2e. We also argue how the evolution of the experimental determination of $R_{D^{(*)}}$ can prove instrumental in falsifying a vector leptoquark explanation of the anomalous B -meson decay data.

1 Introduction

In the Standard Model (SM), charged leptons are only distinguishable due to their masses. In particular, all electroweak couplings to gauge bosons are blind to lepton flavour, leading to an accidental symmetry called lepton flavour universality (LFU), whose validity has been determined to a very high accuracy for instance in $Z \rightarrow \ell^+\ell^-$ and $W^\pm \rightarrow \ell^\pm\nu$ ($\ell = e, \mu, \tau$) decays [1].

However, during the last decade, hints on the violation of LFU in $b \rightarrow c\ell\nu$ and $b \rightarrow s\ell\ell$ decays have begun to emerge, in mounting tension with respect to the SM expectations. In particular, measurements of the “theoretically clean” ratios of branching ratios $R_{D^{(*)}} = \text{BR}(B \rightarrow D^{(*)}\tau\nu)/\text{BR}(B \rightarrow D^{(*)}\ell\nu)$ [2] and $R_{K^{(*)}} = \text{BR}(B \rightarrow K^{(*)}\mu\mu)/\text{BR}(B \rightarrow K^{(*)}ee)$ [3] deviate around $2 - 3\sigma$ from their theoretical predictions, which are, up to phase space suppression, expected to be unity in the SM. Current averages of experimental measurements and the SM predictions can be found in Table 1.

	R_K	R_{K^*}	R_D	R_{D^*}
SM prediction	$\simeq 1$	$\simeq 1$	0.299 ± 0.003	0.258 ± 0.005
Experiment	0.845 ± 0.06	0.69 ± 0.12	0.340 ± 0.030	0.295 ± 0.014

Table 1: SM predictions and (averages of) experimental measurements of the “theoretically clean” LFU observables.

Additionally, measurements of angular observables in $B^{0,+} \rightarrow K^*\mu^+\mu^-$ decays exhibit (local) deviations of $2 - 3\sigma$ in several q^2 bins. These measurements [4] have been recently updated, confirming and strengthening the currently preferred NP hypotheses.

Very recently, the LHCb Collaboration updated ¹ their measurement of $R_K = 0.846_{-0.041}^{+0.044}$ [5] with the deviation to the SM prediction now reaching 3.1σ , thus providing the first *evidence* of LFU violation ².

These curious, persisting tensions with the SM seem to indirectly hint towards the presence of new physics (NP), likely at the TeV-scale. Many different approaches have been explored to identify which (minimal) NP models better succeed in reconciling theoretical predictions with the experimental data. Before addressing the prospects of vector leptoquark (LQ) extensions of the SM (one of the most promising well motivated scenarios to simultaneously explain both anomalies), we will consider a model-independent effective field theory (EFT) based approach. This will allow to generically identify which classes of NP models offer the most appropriate content and interactions to explain the anomalous data.

2 EFT and global fits

The EFT approach relies in parametrising NP effects in terms of higher-order non-renormalisable operators (vestigial traces in the low-energy theory of heavier states, which are integrated out). Starting from the relevant subsets of the effective Lagrangian, cast in terms of the relevant semileptonic Wilson coefficients (WC) $C^{qq';\ell\ell'}$ and effective operators, we comment on how well-motivated scenarios for (sets of) $C^{qq';\ell\ell'}$ become significantly favoured by current data.

The subset of the effective Lagrangian for charged current $d_k \rightarrow u_j \ell \nu_i$ transitions is given by

$$\mathcal{L}_{\text{eff}} \simeq -\frac{4G_F}{\sqrt{2}} V_{jk} \left[(1 + C_{V_L}^{jk\ell i}) (\bar{u}_j \gamma_\mu d_k) (\bar{\ell} \gamma^\mu P_L \nu^i) \right] + \text{H.c.}, \quad (1)$$

where V_{jk} are elements of the Cabibbo-Kobayashi-Maskawa (CKM) quark mixing matrix. While the charged current anomalies $R_{D^{(*)}}$ can be explained with NP contributions to the left-handed vector coefficient $C_{V_L}^{cb\tau\nu}$, the neutral current ones – especially due to the deviations in the angular observables – call upon a dedicated EFT analysis to identify which operator structure (or combination of structures) is preferred by experimental data. A subset of the low energy effective Lagrangian in $b \rightarrow s\ell\ell$ transitions can be cast as

$$\mathcal{L}_{\text{eff}} \simeq \frac{4G_F}{\sqrt{2}} V_{td_j} V_{td_i}^* \left[\frac{\alpha_e}{4\pi} C_9^{ij\ell\ell'} (\bar{d}_i \gamma^\mu P_L d_j) (\bar{\ell} \gamma_\mu \ell') + \frac{\alpha_e}{4\pi} C_{10}^{ij\ell\ell'} (\bar{d}_i \gamma^\mu P_L d_j) (\bar{\ell} \gamma_\mu \gamma_5 \ell') \right]. \quad (2)$$

As it turns out, a very interesting NP scenario is given by considering LFU violating $V - A$ new physics contributions in $\Delta C_9^{bs\mu\mu} = -\Delta C_{10}^{bs\mu\mu}$, in addition to a LFU vector NP contribution denoted by $\Delta C_9^{\text{univ.}}$ which is flavour universal and added to $C_9^{bs\mu\mu}$ and C_9^{bsee} . A fit of all available $b \rightarrow s\ell\ell$ data ³, including the updated measurement in R_K , leads to a $\sim 6.6\sigma$ improvement with respect to the SM prediction. The best fit point is found to be given by $\Delta C_9^{bs\mu\mu} = -0.34_{-0.08}^{+0.08}$ and $\Delta C_9^{\text{univ.}} = -0.74_{-0.17}^{+0.19}$, and shows a $\sim 3\sigma$ preference for non-vanishing NP contributions to the WCs [7], as can be seen by the likelihood contours in the plane of weak effective theories (WET) and SM-EFT Wilson coefficients, shown in the left panel of Figure 1.

Interestingly, and as it has been pointed out in Ref. [8], a universal contribution to $C_9^{bs\ell\ell}$ can be generated from renormalisation group (RG) running from sizeable semi-tauonic operators. In the right panel of Figure 1 we display the likelihood ⁴ contours in the plane of the semi-muonic and semi-tauonic $SU(2)_L$ singlet and triplet SM-EFT Wilson coefficients in $b \rightarrow s\ell\ell$. As can be seen, the

¹Due to an improved determination of the f_s/f_d fragmentation in $B_{(s)}$ -decays LHCb also updated their measurement on $B_{(s)} \rightarrow \mu^+ \mu^-$ decays. However, we have decided to refrain from “digitising” the plots presented on slides, and thus cannot take into account the update in a consistent manner for the present fits.

²For an (animated) overview of how the fit to $b \rightarrow s\ell\ell$ data has evolved upon inclusion of the new measurements see http://moriond.in2p3.fr/2021/EW/slides/ani_fit_evo.mp4.

³For a complete list of observables taken into account, see Appendix B of Ref. [6].

⁴Other than the $b \rightarrow s\ell\ell$ and $R_{D^{(*)}}$ data, the global likelihood also contains the binned branching fractions in exclusive $B \rightarrow D^{(*)} \ell \nu$ decays.

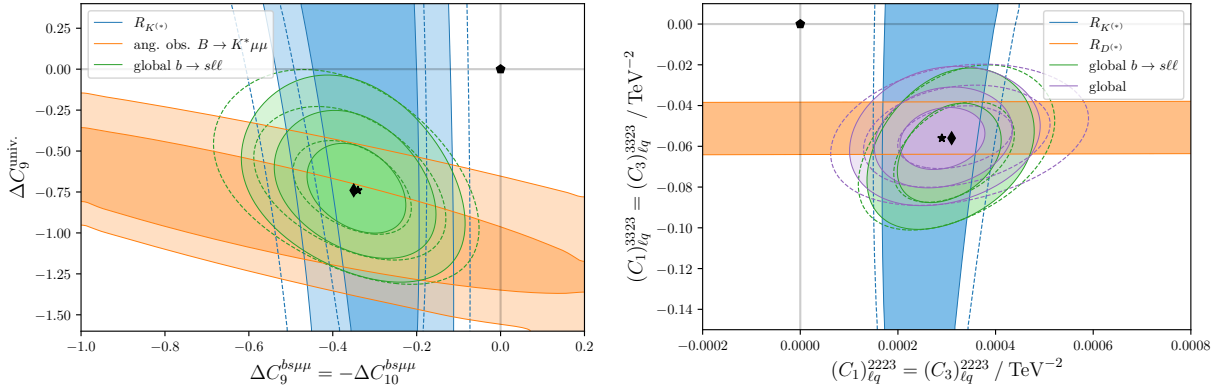


Figure 1: Likelihood contours (1σ , 2σ (and 3σ for the global fit)) in the plane of WET and SM-EFT Wilson coefficients. Dashed contour lines denote the situation prior to the updated 2021 R_K measurement, a pentagon the SM prediction, a diamond the “old” best fit point and a star the new best fit point upon inclusion of the updated R_K data. **Left:** Fit of WET coefficients at 4.8 GeV with the best fit point $\Delta C_9^{bs\mu\mu} = -0.34_{-0.08}^{+0.08}$ and $\Delta C_9^{\text{univ.}} = -0.74_{-0.17}^{+0.19}$. **Right:** Fit of SM-EFT coefficients at 2 TeV with the best fit point of $(C_1)_{\ell q}^{2223} = (2.9_{-0.6}^{+0.6}) \times 10^{-4} \text{ TeV}^{-2}$ and $(C_1)_{\ell q}^{3323} = 0.056_{-0.01}^{+0.01} \text{ TeV}^{-2}$, with a pull of 7.9σ with respect to the SM prediction. Figures taken from Ref. [7].

$b \rightarrow s\ell\ell$ contours are not independent of the semi-tauonic operators, an effect of the RGE-induced universal contributions to $C_9^{bs\ell\ell}$ at the b -quark mass scale.

This correlation between the charged and neutral current anomalies at the high-energy scale strongly hints towards a combined explanation of both tensions in a minimal model. For completeness, in Appendix A we include updates on additional NP hypotheses.

Interestingly, the preferred structure of EFT operators (both in SM-EFT and WET) is naturally generated by the $SU(2)_L$ -singlet vector LQ V_1 , contributing to both charged and neutral current anomalous transitions at the tree-level, while evading stringent constraints from $d_i \rightarrow d_j \nu \bar{\nu}$ decays.

3 Vector leptoquarks

Gauge vector LQs, such as V_1 , naturally arise in (grand) unified theories, specifically from quark-lepton unification, as it occurs in Pati-Salam models. In our study of Ref. [9], and instead of exploring a specific UV completion for V_1 leptoquarks, we chose to find requirements on the couplings of V_1 to the SM fermions in an effective way. The subset of the relevant (left-handed⁵) LQ couplings to SM fermions can be parametrised in a general way as

$$\mathcal{L} \simeq \sum_{i,j,k,l=1}^3 V_1^\mu \left(\bar{d}_L^i \gamma_\mu K_L^{ik} \ell_L^k + \bar{u}_L^j V_{ji}^\dagger \gamma_\mu K_L^{ik} U_{kl}^P \nu_L^l \right) + \text{H.c.}, \quad (3)$$

where K_L^{ij} denote the effective LQ couplings and U^P is the Pontecorvo-Maki-Nakagawa-Sakata (PMNS) leptonic mixing matrix. The matching of the LQ couplings (at the LQ mass scale, $m_{V_1} \simeq 1.5 \text{ TeV}$) to the WCs singled out by the EFT analysis can be done as follows:

$$C_{9,10}^{ij;\ell\ell'} = \mp \frac{\pi}{\sqrt{2} G_F \alpha_{\text{em}} V_{3j} V_{3i}^* m_{V_1}^2} \left(K_L^{i\ell'} K_L^{j\ell'*} \right), \quad C_{jk,\ell i}^{V_L} = \frac{\sqrt{2}}{4 G_F m_{V_1}^2} \frac{1}{V_{jk}} (V K_L U^P)_{ji} K_L^{k\ell*}. \quad (4)$$

In the left panel of Figure 2 we show likelihood contours in the plane of the dominant LQ couplings. Notice that one finds the same correlation between semi-muonic and semi-tauonic couplings in the likelihood contours preferred by $b \rightarrow s\ell\ell$ data as previously encountered in the EFT fits (cf. Figure 1).

⁵Due to the absence of strong hints suggesting non-vanishing right-handed contributions to the WET operators, we restrict the LQ couplings to be left-handed.

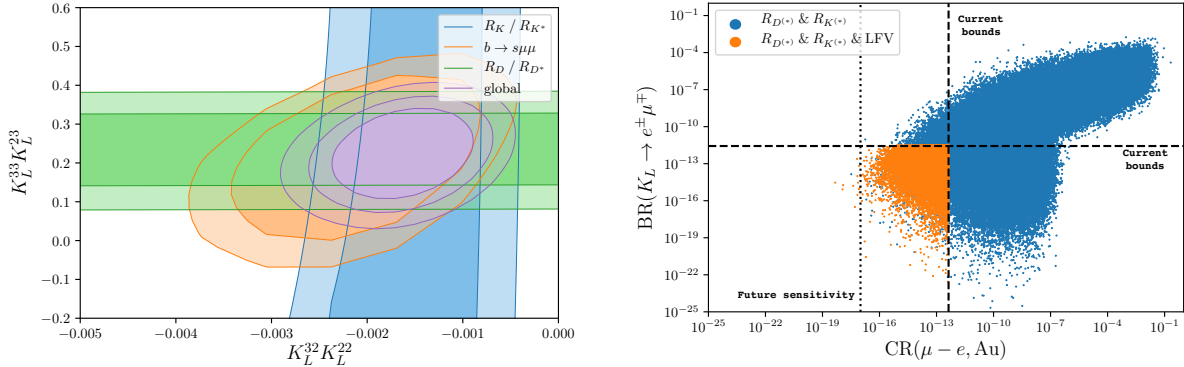


Figure 2: **Left:** Fit of combinations of the dominant V_1 LQ couplings ($K_L^{3i} K_L^{2j}$) to the anomalous data. The likelihood contours correspond to 1σ , 2σ and 3σ . **Right:** Generated Monte-Carlo samples accommodating the B anomalies, displayed in the plane of the two most constraining observables, $\text{CR}(\mu - e, \text{Au})$ and $K_L \rightarrow e^\pm \mu^\mp$. Blue points violate at least one LFV bound while orange points comply with *all* imposed constraints. Figures taken from Ref. [9].

Sizeable V_1 couplings of second- and third-generation quarks to different lepton flavours can lead to strongly enhanced rates in lepton flavour violating (LFV) processes, such as $B \rightarrow K\tau\mu$, which put stringent constraints on the model's parameter space. As we have shown in our analysis in [9], in order to evade those bounds, effectively non-unitary couplings to the SM fermions are necessary. For instance, this can be achieved by introducing vector-like fermions, more specifically vector-like leptons, that mix with the SM fermions. In our approach we have thus parametrised the LQ couplings via 12 unitary rotations incorporating the mixing between the SM leptons and 3 additional generations of vector-like $SU(2)_L$ doublet leptons⁶. In the right panel of Figure 2 we show results of a random scan where we vary the 12 mixing angles in the interval $[-\pi, \pi]$, presenting our results in the plane of the two most constraining LFV observables, namely $K_L \rightarrow \mu^\pm e^\mp$ decays and neutrinoless $\mu - e$ conversion in nuclei. The points displayed (blue) are in agreement with the anomalous data at the 3σ level; however, most of the latter points leads to the violation of at least one experimental LFV bound. Points complying with all imposed constraints (explaining $R_{K,D}^{(*)}$ and respecting all experimental bounds) are marked in yellow. Notice that most of the currently preferred parameter space can be probed by the upcoming experiments COMET and Mu2e [10], both dedicated to searching for neutrinoless $\mu - e$ conversion in Aluminium.

In a second - updated - phenomenological analysis we have now taken the 9 left-handed LQ couplings as independent parameters and we have fit them to more than 350 observables⁷, for three mass benchmark points of $m_{V_1} \in [1.5, 2.5, 3.5]$ TeV; this allows finding a region in the 9-dimensional parameter space in which the B -anomalies can be explained while evading constraints from LFV processes [6]. We assumed the posterior distribution of the couplings to be approximately gaussian and sampled them according their distribution. From the Monte-Carlo samples we have then computed posterior ranges for the observables around the best fit point(s), based on the currently by experimental data preferred parameter space.

Several rare B -decays involving tau-leptons and nnumerous LFV tau-decays are expected to be searched for by the Belle II experiment [11] with improved sensitivities. Due to sizeable couplings of the LQ to b, s - and c -quarks, and to charged leptons, a priori we expect sizeable enhancements

⁶Other representations of vector-like leptons are ruled out since the required mixing pattern would drastically impact Zll couplings already at the tree-level, thus violating experimental bounds on these precisely measured quantities.

⁷These include $b \rightarrow sll$ and $b \rightarrow cl\nu$ data, a large number of lepton flavour violating and conserving (semi-)leptonic (b, c and s) meson and τ decays and several purely leptonic LFV processes. A complete list can be found in Ref. [6].

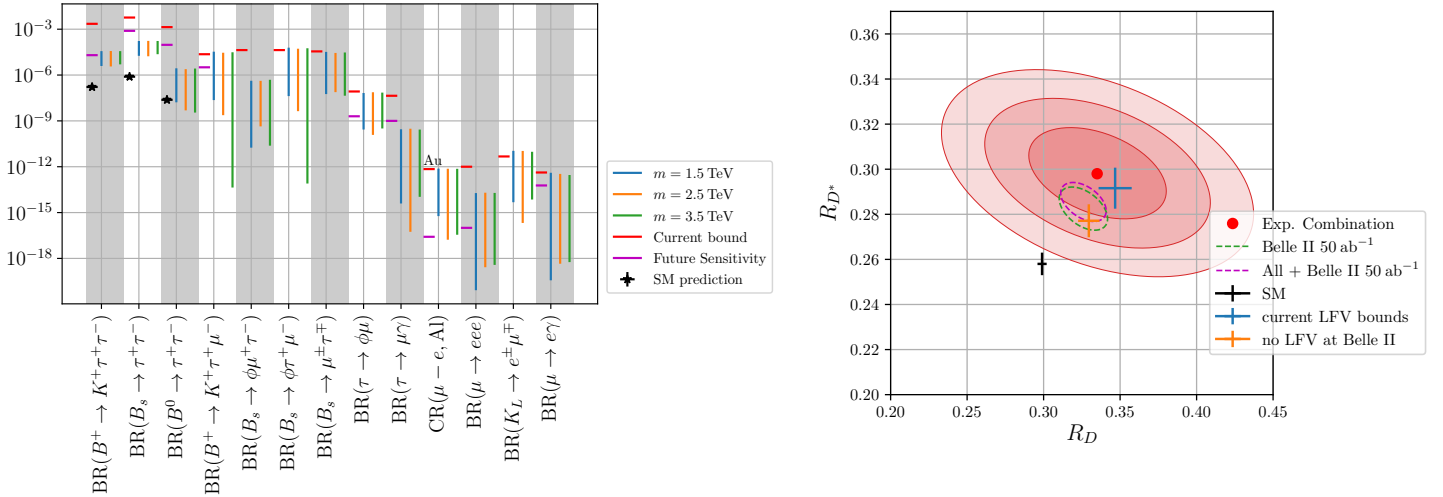


Figure 3: **Left:** Posterior ranges of the vector LQ predictions for several observables searched for by Belle II, COMET and Mu2e. **Right:** Posterior ranges for LQ predictions for $R_{D^{(*)}}$ based on current (future) bounds on LFV processes relevant for the test of the vector LQ hypothesis presented in blue (orange). The predictions for different masses coincide. Also shown are the extrapolations of the current Belle measurement to the sensitivity of Belle II (dashed contourlines). Figures taken from Ref. [6].

of $b \rightarrow s\tau^+\tau^-$ and LFV processes. In the left panel of Figure 3 we show the 1σ ranges of the posterior distributions for several such observables, together with current experimental limits and future sensitivities. In particular, $B \rightarrow K\tau\mu$ and $\tau \rightarrow \phi\mu$ decays are promising channels at Belle II. Additionally, the predicted range of neutrinoless $\mu - e$ in Aluminium will be (almost) fully probed by COMET and Mu2e [10].

The results of this analysis are by no means a guarantee to discover LFV signals in those channels. Thus, we have furthermore studied the impact of *null* results in LFV channels at Belle II, Mu2e and COMET - thus replacing current LFV bounds with future sensitivities in our fit. Results of such a hypothetical future fit are presented in the right panel of Figure 3, where we show predictions of the LQ model for $R_{D^{(*)}}$ based on current and future LFV bounds (blue and orange respectively). Moreover, we have extrapolated the current measurement of $R_{D^{(*)}}$ by Belle to the anticipated accuracy of Belle II with 50 ab^{-1} integrated luminosity, and combined it with all other measurements available, denoted via the green and purple (dashed) ellipses [6]. Curiously, in the absence of LFV signals the LQ expected best fit point (in orange) moves closer to the SM prediction, although overlapping with the 1σ contour of the extrapolated Belle II sensitivity. On the other hand, should future measurements coincide with the central value of the current global average (with improved accuracy), a V_1 -LQ explanation of the $R_{D^{(*)}}$ anomalies would be in conflict with future bounds on LFV processes (again in the absence of any LFV discovery at Belle II). Thus, the evolution of future measurements of $R_{D^{(*)}}$ will prove instrumental in falsifying the vector LQ hypothesis.

4 Conclusion and outlook

In recent years, numerous hints for the presence of LFU violation in charged and neutral current semi-leptonic B -meson decays have emerged in association with several observables. Current EFT analyses appear to favour minimal models that can simultaneously address the tensions in both channels, due to a preference of *universal* contributions to C_9^{bsll} at the b -quark mass scale, which can be induced by RG running effects. This interpretation is further strengthened by the very recently updated measurement of R_K . Following the recent LHCb measurement [5], we have updated fits of several NP hypotheses

leading to a good agreement with the data.

In view of the absence of tree-level couplings between down-type quarks and neutrinos, $SU(2)_L$ -singlet vector LQs are excellent candidates for a combined explanation of the B -meson decay anomalies, although subject to stringent constraints from LFV observables. We have shown that a non-unitary flavour structure of the LQ couplings to SM matter is necessary in order to comply with numerous bounds from flavour observables, which have been measured to be in good agreement with the SM; such a structure can be generated via mixings of SM leptons with heavy vector-like doublet states. We have further explored the flavour phenomenology of this simple vector LQ model, carrying a dedicated statistical analysis; this allowed identifying several “golden modes” that have excellent chances to be observed by upcoming experiments in the near future. Finally, we highlighted the importance of future $R_{D^{(*)}}$ measurements for the model’s viability.

Acknowledgements

JK is indebted to the Organisers of the “55th Rencontres de Moriond” for the kind invitation, and grateful to his collaborators. This project has received support from the European Union’s Horizon 2020 research and innovation programme under the Marie Skłodowska -Curie grant agreement No 860881-HIDDeN.

A Additional updates on global fits

In this Appendix we provide several fit updates on additional NP hypotheses. These results were first presented in the Electroweak Session of the “55th Rencontres de Moriond”, 24 March 2021 [7]. Model-independent fits by other groups have since appeared in [12], while updated studies on V_1 leptoquark scenarios can be found in [13]. All observables taken into account here can be found in Appendix B of Ref. [6].

As a first part of the present update, in Tables 2 and 3 we present our fit’s results for hypotheses with NP contributions present in a single Wilson coefficient, as well as one hypothesis in which we consider 6 Wilson coefficients simultaneously. In order to establish a baseline, we first begin by giving our results prior to and after the inclusion of the updated LHCb measurement of R_K .

	pre Moriond 2021		post Moriond 2021	
WC	BF $\pm 1 \sigma$	Pull _{SM}	BF $\pm 1 \sigma$	Pull _{SM}
$\Delta C_9^{bs\mu\mu}$	-0.94 ± 0.15	5.9	-0.89 ± 0.14	6.3
$\Delta C_{10}^{bs\mu\mu}$	0.50 ± 0.13	4.0	0.52 ± 0.12	4.5
$\Delta C_9^{bs\mu\mu} = -\Delta C_{10}^{bs\mu\mu}$	-0.47 ± 0.09	5.5	$-0.41^{+0.07}_{-0.08}$	5.9

Table 2: Different 1-d NP hypotheses leading to improvements with respect to the SM predictions. The pulls slightly increase upon inclusion of the new R_K measurement.

In the remainder of this appendix we update the fits on NP hypotheses leading to new contributions to two (independent) Wilson coefficients. In contrast to the WET and SM-EFT hypotheses presented in Figure 1, in all of the remaining scenarios $R_{K^*} < R_K$ be accommodated can only be accommodated

	C_9	C_{10}	C'_9	C'_{10}	C_7	C'_7	Pull _{SM}
pre Moriond 2021	$-1.15^{+0.16}_{-0.15}$	$0.17^{+0.15}_{-0.14}$	$0.39^{+0.32}_{-0.33}$	$-0.26^{+0.18}_{-0.17}$	$0.001^{+0.014}_{-0.014}$	$0.005^{+0.014}_{-0.014}$	6.2
post Moriond 2021	$-1.15^{+0.16}_{-0.15}$	$0.17^{+0.15}_{-0.14}$	$0.40^{+0.32}_{-0.33}$	$-0.26^{+0.18}_{-0.17}$	$0.001^{+0.014}_{-0.014}$	$0.005^{+0.014}_{-0.014}$	6.5

Table 3: 6-d NP hypothesis leading to an improvement with respect to the SM predictions. The best fit point mostly remains unaffected, while the significance slightly increases upon inclusion of the new data.

for very specific configurations of the Wilson coefficients. Thus, in Figures 4, 5 and 6 we show in the left panels separate likelihood contours for R_K and R_{K^*} , combining both observables in the right panels. Descriptions of the results, including of the previous and current best fit points with profiled uncertainties, are given in the corresponding captions.

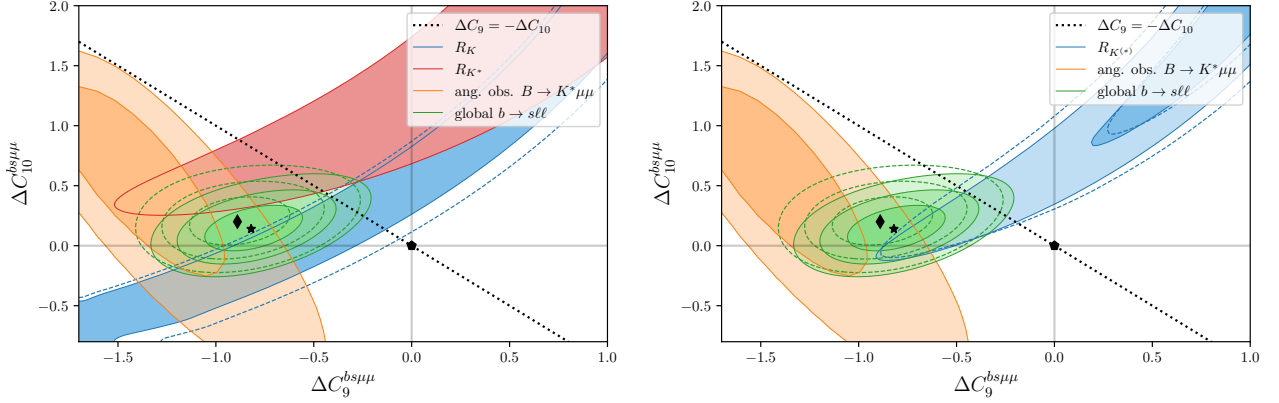


Figure 4: Likelihood contours in the plane of $\Delta C_9^{bs\mu\mu}$ vs. $\Delta C_{10}^{bs\mu\mu}$. The previous best fit point is given by $\Delta C_9^{bs\mu\mu} = -0.89^{+0.17}_{-0.16}$, $\Delta C_{10}^{bs\mu\mu} = 0.20^{+0.13}_{-0.13}$, leading to a pull of 5.8σ . Upon inclusion of the updated R_K measurement, we obtain a new best fit point $\Delta C_9^{bs\mu\mu} = -0.82^{+0.17}_{-0.16}$, $\Delta C_{10}^{bs\mu\mu} = 0.14^{+0.12}_{-0.12}$, leading to a slightly increased pull of 6.2σ . The experimental measurement of $R_{K^*} < R_K$ leads to a slight tension that cannot be fully alleviated. Furthermore, there is a mild tension between $R_{K^{(*)}}$ and the data on the angular observables. Figures taken from Ref. [7].

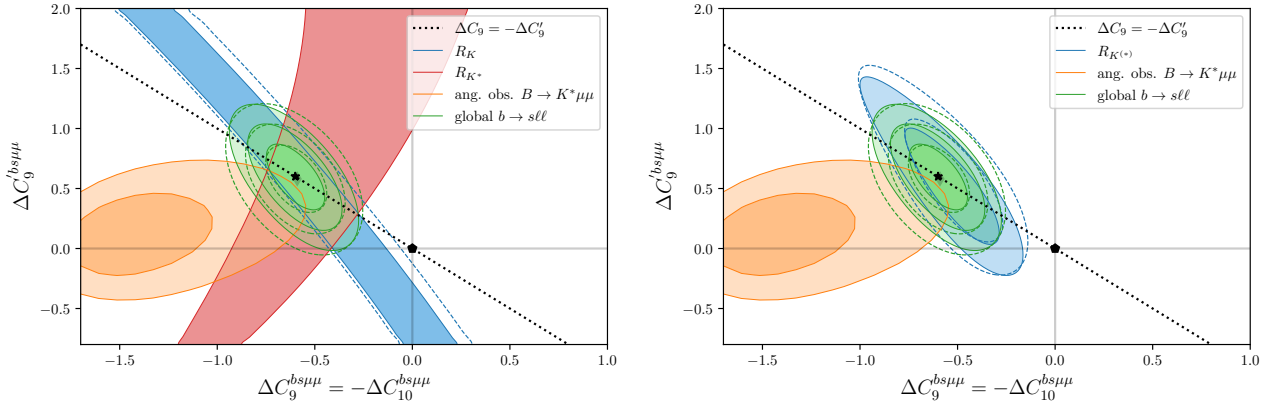


Figure 5: Likelihood contours in the plane of $\Delta C_9^{bs\mu\mu} = -\Delta C_{10}^{bs\mu\mu}$ vs. $\Delta C_9^{bs\mu\mu}$. The previous best fit point is given by $\Delta C_9^{bs\mu\mu} = -0.59^{+0.10}_{-0.10}$, $\Delta C_9^{bs\mu\mu} = 0.58^{+0.18}_{-0.18}$, leading to a pull of 6.0σ . Upon inclusion of the updated R_K measurement, we obtain a new best fit point $\Delta C_9^{bs\mu\mu} = -0.60^{+0.10}_{-0.10}$, $\Delta C_9^{bs\mu\mu} = 0.60^{+0.18}_{-0.18}$, leading to a slightly increased pull of 6.4σ . The experimental measurement of $R_{K^*} < R_K$ can be fully accommodated if $\Delta C_9 \simeq C'_9$. This however leads to a small tension between $R_{K^{(*)}}$ and the angular data. Figures taken from Ref. [7].

References

- [1] P. A. Zyla *et al.* [Particle Data Group], PTEP **2020** (2020) no.8, 083C01.
- [2] G. Caria *et al.* [Belle], Phys. Rev. Lett. **124** (2020) no.16, 161803 [arXiv:1910.05864 [hep-ex]].

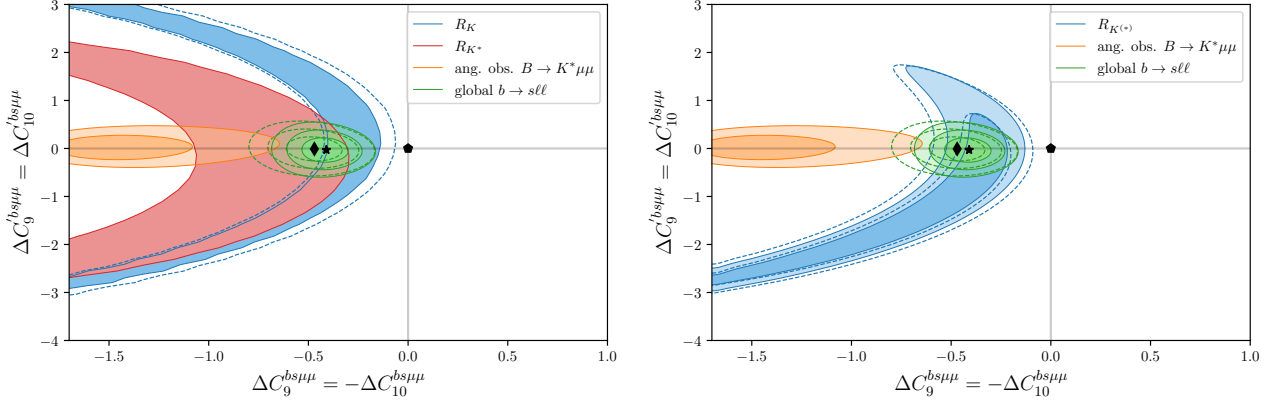


Figure 6: Likelihood contours in the plane of $\Delta C_9^{bs\mu\mu} = \Delta C_{10}^{bs\mu\mu}$ vs. $\Delta C_9^{bs\mu\mu} = -\Delta C_{10}^{bs\mu\mu}$. The previous best fit point is given by $\Delta C_9^{bs\mu\mu} = -0.47_{-0.09}^{+0.09}$, $\Delta C_{10}^{bs\mu\mu} = -0.01_{-0.16}^{+0.17}$, leading to a pull of 5.8σ . Upon inclusion of the updated R_K measurement, we obtain a new best fit point $\Delta C_9^{bs\mu\mu} = -0.41_{-0.08}^{+0.07}$, $\Delta C_{10}^{bs\mu\mu} = -0.03_{-0.16}^{+0.17}$, leading to a slightly *decreased* pull of 5.5σ . The tensions between R_K and R_{K^*} , and R_K and the angular data, increases due to the improved accuracy in the experimental measurement of R_K , hence leading to a decreased pull. Figures taken from Ref. [7].

- [3] R. Aaij *et al.* [LHCb], Phys. Rev. Lett. **122** (2019) no.19, 191801 [arXiv:1903.09252 [hep-ex]]; R. Aaij *et al.* [LHCb], JHEP **08** (2017), 055 [arXiv:1705.05802 [hep-ex]].
- [4] R. Aaij *et al.* [LHCb], JHEP **02** (2016), 104 [arXiv:1512.04442 [hep-ex]]; R. Aaij *et al.* [LHCb], Phys. Rev. Lett. **125** (2020) no.1, 011802 [arXiv:2003.04831 [hep-ex]]; R. Aaij *et al.* [LHCb], arXiv:2012.13241 [hep-ex].
- [5] R. Aaij *et al.* [LHCb], arXiv:2103.11769 [hep-ex].
- [6] C. Hati, J. Kriewald, J. Orloff, A. M. Teixeira, “The fate of vector leptoquarks: impact of future flavour data,” arXiv:2012.05883 [hep-ph].
- [7] J. Kriewald, Presentation at the “55th Rencontres de Moriond”, 24 March 2021 http://moriond.in2p3.fr/2021/EW/slides/3_flavour_03_kriewald.pdf
- [8] A. Crivellin, C. Greub, D. Müller and F. Saturnino, Phys. Rev. Lett. **122** (2019) no.1, 011805 [arXiv:1807.02068 [hep-ph]].
- [9] C. Hati, J. Kriewald, J. Orloff and A. M. Teixeira, JHEP **12** (2019), 006 [arXiv:1907.05511 [hep-ph]].
- [10] R. Abramishvili *et al.* [COMET], PTEP **2020** (2020) no.3, 033C01 [arXiv:1812.09018 [physics.ins-det]]; L. Bartoszek *et al.* [Mu2e], “Mu2e Technical Design Report,” arXiv:1501.05241 [physics.ins-det].
- [11] E. Kou *et al.* [Belle II], PTEP **2019** (2019) no.12, 123C01 [erratum: PTEP **2020** (2020) no.2, 029201] [arXiv:1808.10567 [hep-ex]].
- [12] L. S. Geng, B. Grinstein, S. Jäger, S. Y. Li, J. Martin Camalich and R. X. Shi, arXiv:2103.12738 [hep-ph]; W. Altmannshofer and P. Stangl, arXiv:2103.13370 [hep-ph].
- [13] A. Angelescu, D. Bećirević, D. A. Faroughy, F. Jaffredo and O. Sumensari, arXiv:2103.12504 [hep-ph]; G. Hiller, D. Loose and I. Nišandžić, arXiv:2103.12724 [hep-ph]; C. Cornella, D. A. Faroughy, J. Fuentes-Martín, G. Isidori and M. Neubert, arXiv:2103.16558 [hep-ph].